

Best-Fit Ellipsoids of Atom-Probe Tomographic Data to Study Coalescence of γ' ($L1_2$) Precipitates in Ni-Al-Cr

Richard A. Karnesky^{a,*} Chantal K. Sudbrack^a
David N. Seidman^{a,b}

^a*Department of Materials Science and Engineering, Northwestern University,
Evanston, IL 60208–3108, USA*

^b*Northwestern University Center for Atom-Probe Tomography (NUCAPT),
Evanston, IL 60208–3108, USA*

Abstract

An algorithm is presented to fit precipitates in atom probe tomographic data sets as equivalent ellipsoids. Unlike previous techniques, which measure only the radius of gyration, these ellipsoids retain the moments of inertia and principle axes of the original precipitate, preserving crystallographic orientational information. The algorithm is applied to study interconnected γ' -precipitates ($L1_2$) in the γ -matrix (FCC) of a Ni-Al-Cr alloy. The precipitates are found to coagulate along $\langle 110 \rangle$ -type directions.

Key words: Best-fit ellipsoid, Atom-probe tomography, Coarsening, Nickel alloys

* Corresponding author.

Email address: karnesky@northwestern.edu (Richard A. Karnesky).

URL: <http://arc.nucapt.northwestern.edu/> (Richard A. Karnesky).

One of the principle challenges that analyzing three-dimensional atom-probe tomographic (APT) results poses is the amount of raw data that the instruments are now able to collect [1,2]; we have collected continuous data sets as large as 2.1×10^8 properly ranged atoms from a single specimen. It is necessary to extract information about spatial and compositional measures, such as precipitate size from these data sets. A common method to measure the size of precipitates is to calculate a single radius of gyration (or, from this, the Guinier radius) [3,4]. While this technique works well for equiaxed, spheroidal precipitates [5,6], many alloy systems investigated by APT have non-spherical features [7,8,9,10,11,12,13,14,15]. The radius of gyration technique does not, however, retain three-dimensional information concerning precipitate orientation.

In this article, a more general alternative to the radius of gyration is presented and applied. Best-fit ellipsoids have equivalent centroids, moments of inertia, and principle axes for arbitrarily shaped precipitates. The crystallographic orientations of the resulting ellipsoids are then used to study the coagulation-coalescence coarsening mechanism in a Ni-Al-Cr alloy, which occurs when the γ' -precipitate number density is large ($> 10^{24} \text{ m}^{-3}$) and the edge-to-edge distance between adjacent γ' -precipitates is small ($< 2 \text{ nm}$) [16,17].

In lattice kinetic Monte Carlo simulations, a coagulation-coalescence coarsening mechanism is reported [17]. This mechanism is caused by non-equilibrium overlapping diffusion fields, which originate from the long-range vacancy-solute binding energies and a small mean edge-to-edge interprecipitate distance. The non-equilibrium concentration profiles observed at the γ' -precipitate/ γ -matrix interfaces lead to a higher interfacial free energy than for fully equilibrated γ' -precipitates. The excess free energy of the region of overlapping concentration profiles (“diffuse neck”) can decrease by changing the concentration thereof into a well-formed neck [17]. Phase-field simulations find that the rate of γ' -precipitate coalescence is increased when the γ/γ' -interfacial width is increased artificially, thereby increasing the overlapping diffusion fields [18]. While nanometer-sized coagulated γ' -precipitates might have been observed experimentally, past studies only commented on whether precipitates appeared to be non-equiaxed [19,20,21], necked [22,23], or chemically ordered [16]. They did not explore the crystallographic orientation for precipitate coagulation.

A Ni-5.2 Al-14.2 Cr (at.%) alloy was melted under an Ar atmosphere and chill cast. Its chemical composition was verified by inductively coupled plasma spectroscopy. The alloy was homogenized for 24 h at 1300°C, which resulted in coarse grains (0.5–2 mm diameter). After homogenization, the alloy was annealed at 900°C (γ -phase field) and water quenched to ambient temperature. The solutionized alloy was sectioned and aged for 4 h at 600°C and then quenched. This treatment leads to the greatest percentage of γ' -precipitates that are interconnected by necks ($30 \pm 4\%$) [16]. The specimens were cut,

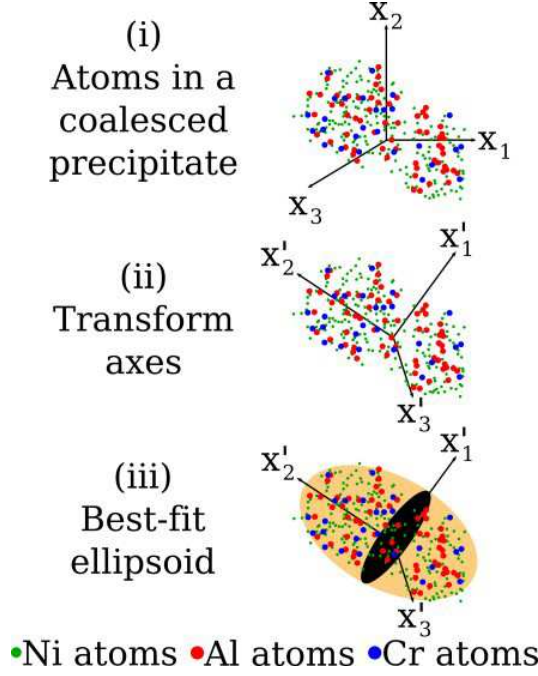


Fig. 1. The best-fit ellipsoid of a precipitate is determined in three steps: (i) for a reference set of axes (X_1 , X_2 , and X_3), identify the x_1 , x_2 , x_3 coordinates of all atoms in a precipitate and its center of mass to obtain a moment of inertia tensor (L) (Eqs. 1–3); (ii) the orientation of the principle axes (X'_1 , X'_2 , and X'_3) of the ellipsoid axes construct a Jacobian transformation matrix that will diagonalize L . (iii) the lengths of the major and minor semi-axes of the best-fit ellipsoid are found from the eigenvalues of the transformed matrix. (Eq. 4).

ground, and then electropolished into APT tips. Three separate APT runs of ca. 3×10^6 atoms were collected on a first-generation 3-D APT [24,25] at a specimen temperature of 40.0 ± 0.3 K, a pulse fraction of 19%, and a pulse repetition rate of 1.5 kHz. The computer programs IVAS (Imago Scientific Instruments) and ADAM [26] were used to analyze APT data. The γ/γ' interface is delineated using a 9 at.% Al isoconcentration surface [27] and the atoms contained within the γ' -surface were exported and segmented into individual γ' -precipitates by a modified envelope algorithm [3,4,28,29].

The γ' -precipitates are divided into three classes: (i) single γ' -precipitates (uncoagulated, without a concave neck) that are not cut by the surface of the analyzed volume; (ii) two or more coalesced γ' -precipitates that are interconnected by a concave neck; (iii) γ' -precipitates cut by the analysis volume boundary. Class (i) accounts for 42% of γ' -precipitates analyzed, class (ii) accounts for 28% of the γ' -precipitates analyzed, and only 12% of them are formations of more than two γ' -precipitates (the largest of which is made up of five distinguishable γ' -precipitates). The best-fit ellipsoid method yields quantitative results for all three classes; particularly class (ii), which is important for understanding the coagulation-coalescence mechanism of γ' -precipitate coarsening.

A schematic that explains the fitting of an equivalent ellipsoid to atoms of coagulated and coalesced precipitates is presented in Fig. 1. For a reference space defined by Cartesian axes X_1, X_2, X_3 (typically the analysis direction and the two orthogonal principle directions of the area detector), the major and minor axes of the best-fit ellipsoid of a precipitate containing N atoms are determined directly from its eigenvalues $(\lambda_1, \lambda_2, \lambda_3)$, also referred to as the principle axes [30]. The principle axes are segments along the transformed Cartesian X'_1, X'_2 , and X'_3 axes and are obtained from the diagonalization of the characteristic length matrix, L (also known as the inertia tensor). This diagonalization is obtained by a Jacobian transformation [31] of a symmetric second-rank tensor, as follows:

$$L = \begin{bmatrix} l_{11} & l_{12} & l_{13} \\ l_{12} & l_{22} & l_{23} \\ l_{13} & l_{23} & l_{33} \end{bmatrix} \xrightarrow{\text{transform}} \begin{bmatrix} \lambda_1 & 0 & 0 \\ 0 & \lambda_2 & 0 \\ 0 & 0 & \lambda_3 \end{bmatrix}; \quad (1)$$

where the characteristic lengths, l_{jk} , are calculated from the positions of i^{th} atom in the reference space ($x_1(i)$, $x_2(i)$, and $x_3(i)$), relative to a precipitate's center of mass ($x_1(\text{com})$, $x_2(\text{com})$, and, $x_3(\text{com})$), averaged over N atoms, employing:

$$l_{kk} = \frac{1}{N} \sum_i^N \left(\sum_{j \neq k} (x_j(i) - x_j(\text{com}))^2 \right) \quad (2)$$

$$l_{jk} = -\frac{1}{N} \sum_i^N ((x_j(i) - x_j(\text{com}))(x_k(i) - x_k(\text{com}))) \quad \text{for } j \neq k \quad (3)$$

The diagonalization of the L matrix follows a procedure outlined in Ref. [31]. The transformation matrix used for this diagonalization yields the orientation of the ellipsoid with respect to the reference state. Defining $\lambda_1 \geq \lambda_2 \geq \lambda_3$, the semi-axes (S_i) of the best-fit ellipsoid are given by:

$$S_i = \sqrt{\frac{5}{2} (\lambda_j + \lambda_k - \lambda_i)} \quad \text{for } j \neq k; \quad (4)$$

where $S_3 \geq S_2 \geq S_1$ are the major semi-axis and two minor semi-axes, respectively.

Figure 2 shows a reconstruction of one APT data set where ellipsoids have been

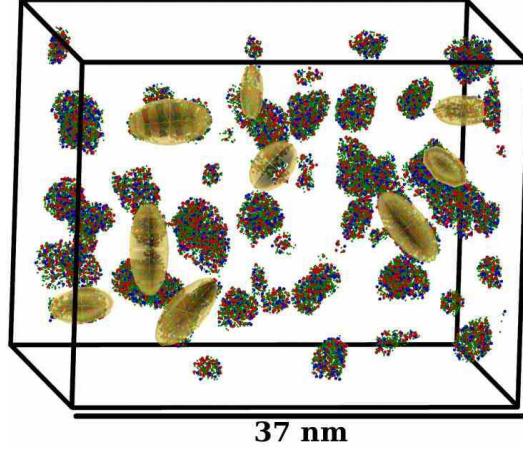


Fig. 2. A representative data set for a Ni-5.2 Al-14.2 Cr (at.%) alloy, whose thermal history is discussed in the text. The coloring scheme matches that of Fig. 1, with Ni atoms in green, Al atoms in red, and Cr atoms in blue. The atoms in the γ -matrix (FCC) are omitted for clarity. The gold colored best-fit ellipsoids indicate those γ' ($L1_2$) precipitates that are interconnected by necks.

fit to interconnected γ' -precipitates. As is seen, the best-fit ellipsoid retains 3-D size and crystallographic orientation information that is jettisoned by other techniques [3,4].

Single γ' -precipitates that are not cut by the analysis volume have aspect ratios of $\frac{S_3}{S_2} = 1.5 \pm 0.5$ and $\frac{S_2}{S_1} = 1.3 \pm 0.2$. The closeness of these values to unity is consistent with equiaxed, uncoagulated precipitates.

Coalesced γ' -precipitates that are interconnected by necks have aspect ratios of $\frac{S_3}{S_2} = 2.9 \pm 0.9$ and $\frac{S_2}{S_1} = 1.3 \pm 0.3$. The ratio for $\frac{S_3}{S_2}$ is about twice the same ratio for uncoagulated precipitates, but $\frac{S_2}{S_1}$ is about the same for the two classes. This demonstrates that a majority of these consist of two equiaxed γ' -precipitates that have coagulated and undergone coalescence.

Single γ' -precipitates that are cut by the edge of the analysis volume can serve as a check of the best-fit ellipsoid method. These have $\frac{S_3}{S_2} = 2.2 \pm 0.8$ and $\frac{S_2}{S_1} = 1.4 \pm 0.4$ because the equiaxed, uncoagulated γ' -particles are, on average, cut in two by the analysis boundary.

It is useful to relate the axes of the analysis volume with specific crystallographic directions to study the orientation of γ' -precipitate coagulation. The analysis direction, which was chosen near the 002 crystallographic pole, provides us with the [001] direction. The [010] and [100] directions can be deduced from a field-ion micrograph (Fig. 3). The edges of the square formed by connecting the 113 family of poles are $\langle 100 \rangle$ -type directions [32]. The angles between these edges and those edges of the APT analysis area are measured and averaged. The analysis volume is then rotated about the [100] analysis

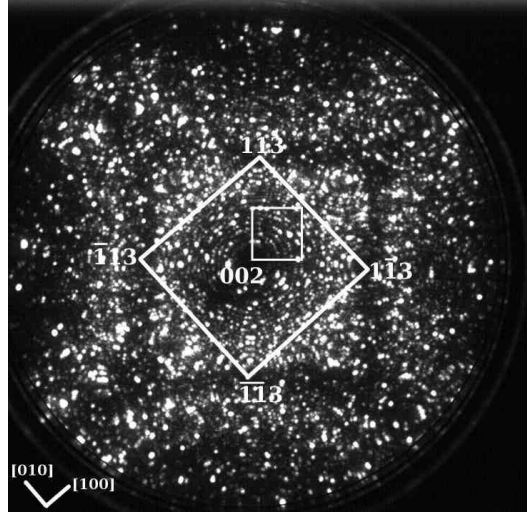


Fig. 3. An FIM image, centered on the 002 pole, taken before APT analysis. The small square denotes the area and orientation for the data set in Fig. 1. The larger square connects the 113 family of poles and the edges of this square give the $[010]$ and $[100]$ directions.

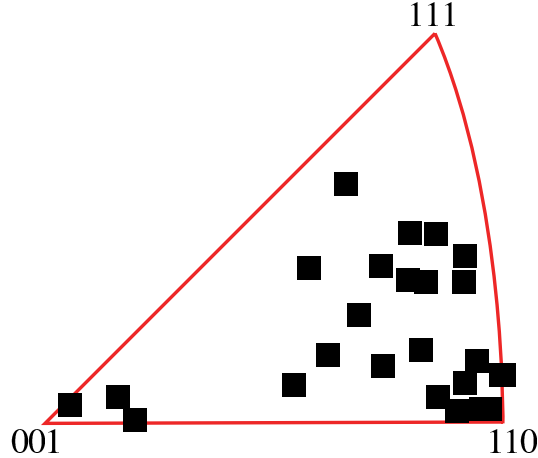


Fig. 4. An inverse pole figure for all interconnected γ' ($L1_2$) precipitates in this study, presented in the standard stereographic triangle. There is a preference for coagulation along and close to $\langle 110 \rangle$ -type directions, which is consistent with a diffusion controlled mechanism for coagulation.

direction by this amount. One standard deviation of this measurement of four angles is $1\text{--}4^\circ$ for the three data sets.

The rotation matrix used in the best-fit ellipsoid method yields the Bunge Euler angles [33] for the major principle axis of the γ' -precipitate with respect to this crystallographically-resolved reference system. From these, an inverse pole figure (Fig. 4) shows the orientations of γ' -precipitates that are the result of the coagulation-coalescence coarsening. There is a preference for coagulation along the $\langle 110 \rangle$ -type directions. 30% of the coalesced precipitates

are within 10° and 71% are within 15° of $\langle 110 \rangle$ -type directions. In the FCC structure of the γ -matrix, $\langle 110 \rangle$ is the fastest diffusion path for solute clusters, and is therefore consistent with the model presented in Ref. [17]. Some γ' -precipitates coagulated along $\langle 100 \rangle$, which is the next-fastest diffusion path and none coagulated along $\langle 111 \rangle$, which is a slower path.

No crystallographic orientational preference was found for single, uncoagulated γ' -precipitates. This supports, once more, the equiaxed nature of γ' -precipitates and the proper reconstruction approach for analyzing the raw APT data. The γ' -precipitates that are cut by the analysis boundary show a preference for the $[100]$ direction, as that direction makes up the majority of the analysis frustum's surface.

The measurement of size and orientation of non-spheroidal precipitates in APT data requires more spatial information to be preserved than for the commonly used methods currently reported to date. We have demonstrated that the best-fit ellipsoid technique preserves the center of gravity, moment of inertia, and principle axes of any precipitate. The technique is applied to specific results for a Ni-Al-Cr alloy with both uncoagulated equiaxed γ' -precipitates and nonequiaxed lobed precipitates that formed through a coagulation-coalescence coarsening mechanism.

Acknowledgements

This research is supported by the National Science Foundation, Division of Materials Research, under contract DMR-0241928. RAK received partial support from a Walter P. Murphy (WPM) Fellowship and the US Department of Energy (DE-FG02-98ER45721). CKS received partial support from an NSF graduate research fellowship, a WPM Fellowship, and a Northwestern University terminal year fellowship. We thank Imago Scientific Instruments and Dr. M. K. Miller for permitting RAK to modify the source code for ENVELOPE, and Dr. D. Mainprice for his inverse pole figure software, IPF2K. Prof. D. C. Dunand, Dr. Z. Mao, and Dr. G. Martin are thanked for discussions.

References

- [1] T. F. Kelly, M. K. Miller, Atom probe tomography, *Review of Scientific Instruments* 78 (3).
- [2] D. N. Seidman, Three-dimensional atom-probe tomography: Advances and applications, *Annual Review of Materials Research* 37 (2007) 127–158.

- [3] M. K. Miller, Atom Probe Tomography: Analysis at the Atomic Level, Kluwer Academic/Plenum, New York, 2000.
- [4] M. K. Miller, E. A. Kenik, Atom probe tomography: A technique for nanoscale characterization, *Microscopy and Microanalysis* 10 (2004) 336–341.
- [5] M. K. Miller, B. D. Wirth, G. R. Odette, Precipitation in neutron-irradiated Fe-Cu and Fe-Cu-Mn model alloys: a comparison of APT and SANS data, *Materials Science and Engineering A* 353 (2003) 133–139.
- [6] R. P. Kolli, D. N. Seidman, Comparison of compositional and morphological atom-probe tomography analyses for a multicomponent Fe-Cu steel
Submitted.

URL <http://nucapt.northwestern.edu/refbase/show.php?record=713>
- [7] F. Soisson, A. Barbu, G. Martin, Monte Carlo simulations of copper precipitation in dilute iron-copper alloys during thermal ageing and under electron irradiation, *Acta Materialia* 44 (1996) 3789–3800.
- [8] E. Cadel, D. Lemarchand, S. Chambrelaud, D. Blavette, Atom probe tomography investigation of the microstructure of superalloys N18, *Acta Materialia* 50 (2002) 957–966.
- [9] A. Heinrich, T. Al-Kassab, R. Kirchheim, Investigation of the early stages of decomposition of Cu–0.7at.% Fe with the tomographic atom probe, *Materials Science and Engineering A* 353 (2003) 92–98.
- [10] D. Wolde-Giorgis, T. Al-Kassab, R. Kirchheim, Nucleation and growth in Cu–0.7at.% Ti as studied with the tomographic atom probe, *Materials Science and Engineering A* A353 (2003) 152–157.
- [11] M. Dumont, W. Lefebvre, B. Doisneau-Cottignies, A. Deschamps, Characterisation of the composition and volume fraction of η' and η precipitates in an Al-Zn-Mg alloy by a combination of atom probe, small-angle X-ray scattering and transmission electron microscopy, *Acta Materialia* 53 (2005) 2881–2892.
- [12] D. Isheim, G. Hsieh, R. D. Noebe, D. N. Seidman, Nanostructural temporal evolution and solute partitioning in model Ni-based superalloys containing ruthenium, rhenium, and tungsten, in: J. M. Howe, D. E. Laughlin, J. K. Lee, D. J. Srolovitz, U. Dahmen, W. A. Soffa (Eds.), *Solid-Solid Phase Transformations in Inorganic Materials*, Vol. 1, TMS, Warrendale, PA, 2005, pp. 309–314.

URL <http://nucapt.northwestern.edu/refbase/show.php?record=187>
- [13] S. D. Erlach, H. Leitner, M. Bischof, H. Clemens, F. Danoix, D. Lemarchand, I. Siller, Comparison of NiAl precipitation in a medium carbon secondary hardening steel and C-free PH13-8 maraging steel, *Materials Science and Engineering: A* 429 (2006) 96–106.

- [14] E. V. Pereloma, I. B. Timokhina, K. F. Russell, M. K. Miller, Characterization of clusters and ultrafine precipitates in Nb-containing C-Mn-Si steels, *Scripta Materialia* 54 (2006) 471–476.
- [15] A. Andersson, K. Stiller, M. Hättestrand, Comparison of early stages of precipitation in Mo-rich and Mo-poor maraging stainless steels, *Surface and Interface Analysis* 39 (2007) 195–200.
- [16] C. K. Sudbrack, K. E. Yoon, R. D. Noebe, D. N. Seidman, Temporal evolution of the nanostructure and phase compositions in a model Ni-Al-Cr alloy, *Acta Materialia* 54 (2006) 3199–3210.
- [17] Z. Mao, C. K. Sudbrack, K. E. Yoon, G. Martin, D. N. Seidman, The mechanism of morphogenesis in a phase separating concentrated multi-component alloy, *Nature Materials* 6 (2007) 210–216.
- [18] J. Z. Zhu, T. Wang, A. J. Ardell, S. H. Zhou, Z. K. Liu, L. Q. Chen, Three-dimensional phase-field simulations of coarsening kinetics of γ' particles in binary Ni-Al alloys, *Acta Materialia* 52 (2004) 2837–2845.
- [19] R. E. Beddoe, P. Haasen, G. Kostorz, Early stages of decomposition in Ni-Al single crystals studied by small-angle neutron scattering, in: P. Haasen, V. Gerold, R. Wagner, M. F. Ashby (Eds.), *Decomposition of Alloys: The Early Stages*, Vol. 2 of *Acta-Scripta Metallurgica Proceedings Series*, Pergamon, Oxford, 1984, pp. 233–238.
- [20] C. Schmuck, F. Danoix, P. Caron, A. Hauet, D. Blavette, Atomic scale investigation of ordering and precipitation processes in a model Ni-Cr-Al alloy, *Applied Surface Science* 94–95 (1996) 273–279.
- [21] C. K. Sudbrack, K. E. Yoon, R. D. Noebe, D. N. Seidman, The temporal evolution of the nanostructure of a model Ni-Al-Cr superalloy, *TMS Letters* 1 (2004) 25–26.
URL <http://nucapt.northwestern.edu/refbase/show.php?record=199>
- [22] C. K. Sudbrack, R. D. Noebe, D. N. Seidman, Temporal evolution of sub-nanometer compositional profiles across the γ/γ' interface in a model Ni-Al-Cr superalloy, in: J. M. Howe, D. E. Laughlin, J. K. Lee, D. J. Srolovitz, U. Dahmen, W. A. Soffa (Eds.), *Solid-Solid Phase Transformations in Inorganic Materials*, Vol. 2, TMS, Warrendale, PA, 2005, pp. 543–548.
URL <http://nucapt.northwestern.edu/refbase/show.php?record=180>
- [23] C. K. Sudbrack, R. D. Noebe, D. N. Seidman, Compositional pathways and capillary effects during isothermal precipitation in a nondilute Ni-Al-Cr alloy, *Acta Materialia* 55 (2007) 119–130.
- [24] D. Blavette, B. Deconihout, A. Bostel, J. M. Sarrau, M. Bouet, A. Menand, The tomographic atom probe: A quantitative three-dimensional nanoanalytical instrument on an atomic scale, *Review of Scientific Instruments* 64 (1993) 2911–2919.

- [25] A. Cerezo, T. J. Godfrey, S. J. Sijbrandij, G. D. W. Smith, P. J. Warren, Performance of an energy-compensated three-dimensional atom probe, *Review of Scientific Instruments* 69 (1998) 49–58.
- [26] O. Hellman, J. Vandenbroucke, J. Blatz du Rivage, D. N. Seidman, Application software for data analysis for three-dimensional atom probe microscopy, *Materials Science and Engineering A* 327 (2002) 29–33.
- [27] O. C. Hellman, J. Blatz du Rivage, D. N. Seidman, Efficient sampling for three-dimensional atom probe microscopy data, *Ultramicroscopy* 95 (2003) 199–205.
- [28] J. M. Hyde, C. A. English, An analysis of the structure of irradiation Cu-enriched clusters in low and high nickel welds, in: G. E. Lucas, L. Snead, M. A. Kirk, R. G. Ellman (Eds.), *Microstructural Processes in Irradiated Materials–2000*, Vol. 650 of *Materials Research Society Symposia Proceedings*, Materials Research Society, Warrendale, PA, 2001, pp. R.6.6.1–12.
- [29] E. A. Marquis, Microstructural evolution and strengthening mechanisms in Al-Sc and Al-Mg-Sc alloys, Ph.D. thesis, Northwestern University (2002).
URL <http://nucapt.northwestern.edu/refbase/show.php?record=151>
- [30] J. F. Nye, *Physical Properties of Crystals: Their Representation by Tensors and Matrices*, Oxford University Press, Oxford, 1985.
- [31] W. H. Press, S. A. Teukolsky, W. T. Vetterling, B. P. Flannery, *Numerical Recipes: The Art of Scientific Computing*, 1st Edition, Cambridge University Press, Cambridge, 1986.
- [32] K. M. Bowkett, D. A. Smith, *Field-Ion Microscopy*, North-Holland, Amsterdam, 1970.
- [33] H. J. Bunge, *Texture Analysis in Materials Science: Mathematical Methods*, Butterworths, Boston, 1982.